EARTHQUAKE ENGINEERING AND STRUCTURAL DYNAMICS
Earthquake Engng Struct. Dyn. 2007; **36**:1255–1273
Published online 27 February 2007 in Wiley InterScience (www.interscience.wiley.com). DOI: 10.1002/eqe.681

Full-scale experimental verification of resetable semi-active stiffness dampers

J. N. Yang[1,*,†], J. Bobrow[2], F. Jabbari[2], J. Leavitt[2], C. P. Cheng[3] and P. Y. Lin[3]

[1]*Department of Civil and Environmental Engineering, University of California, Irvine, CA 92697, U.S.A.*
[2]*Department of Mechanical and Aerospace Engineering, University of California, Irvine, CA 92697, U.S.A.*
[3]*National Center for Research on Earthquake Engineering, Taipei, Taiwan*

SUMMARY

Because of many advantages over other control systems, semi-active control devices have received considerable attention for applications to civil infrastructures. A variety of different semi-active control devices have been studied for applications to buildings and bridges subject to strong winds and earthquakes. Recently, a new semi-active control device, referred to as the resetable semi-active stiffness damper (RSASD), has been proposed and studied at the University of California, Irvine (UCI). It has been demonstrated by simulation results that such a RSASD is quite effective in protecting civil engineering structures against earthquakes, including detrimental near-field earthquakes. In this paper, full-scale hardware for RSASD is designed and manufactured using pressurized gas. Experimental tests on full-scale RSASDs have been conducted to verify the hysteretic behaviours (energy dissipation characteristics) and the relation between the damper stiffness and the gas pressure. The correlation between the experimental results of the hysteresis loops of RASADs and that of the theoretical ones has been assessed qualitatively. Experimental results further show the linear relation between the gas pressure and the stiffness of the RSASD as theoretically predicted. Finally, shake table tests have also been conducted using an almost full-scale 3-storey steel frame model equipped with full-scale RSASDs at the National Center for Research on Earthquake Engineering (NCREE), Taipei, Taiwan, and the results are presented. Experimental results demonstrate the performance of RSASDs in reducing the responses of the large-scale building model subject to several near-field earthquakes. Copyright © 2007 John Wiley & Sons, Ltd.

Received 13 June 2006; Revised 20 November 2006; Accepted 12 January 2007

KEY WORDS: structural control; semi-active stiffness damper; near-field earthquake; hysteresis loop; full-scale device; shake table test

*Correspondence to: J. N. Yang, Department of Civil and Environmental Engineering, University of California, Irvine, CA 92697, U.S.A.
†E-mail: jnyang@uci.edu

Contract/grant sponsor: US National Science Foundation; contract/grant number: CMS-0218813

1. INTRODUCTION

Passive, active, semi-active and hybrid control systems offer alternative means to protect structures against natural hazards, such as earthquakes, strong winds, etc. Because of their mechanical simplicity, low-power requirements, and large and controllable force capacity, semi-active control systems are particularly attractive and have received considerable attention recently for applications to civil infrastructures. Semi-active control strategies may offer the reliability of passive devices with better performance, and maintain much of the versatility and adaptability of active control systems without requiring large power sources. Various types of semi-active control devices have been proposed in the literature as described in, e.g. [1–21]. These semi-active control systems include, for instance, variable-orifice fluid dampers, e.g. [3–6], controllable fluid dampers such as MR dampers, e.g. [7], controllable friction dampers, e.g. [8–10], variable stiffness devices, e.g. [11, 12, 20, 21], resetable semi-active stiffness dampers (RSASD), e.g. [13–16], etc.

Recently, the RSASD has been proposed and studied for possible application to civil engineering structures subject to natural hazards, e.g. [9, 13–16]. It has been demonstrated, through extensive simulations, that the RSASD is quite effective in reducing the responses of buildings [14, 15] and bridges [9] subject to earthquakes. Likewise, it can be used in conjunction with a base isolation system to reduce the response of buildings subject to detrimental near-field earthquakes [16]. However, to date, full-scale RSASDs have not been built and shake table tests on large-scale structures have not been conducted. In this paper, full-scale RSASDs, designed and manufactured at the University of California at Irvine (UCI) using pressurized gas rather than liquid, will be presented. The advantage of using pressurized gas is the ease of achieving the desirable stiffness without an accumulator. Additionally, the stiffness of the RSASD can be adjusted easily by changing the gas pressure.

The energy dissipation capacity of any control device is reflected by the hysteresis loop of the device, because the area bounded by the hysteresis loop is the energy dissipated by the device in one cycle. Hence, the bigger the hysteresis loop of a device is, the better the energy dissipation capability will be. Experimental tests of the full-scale RSASD have been conducted, by connecting them to a large actuator and subjecting them to sinusoidal loading, to generate the experimental hysteresis loops and to obtain the stiffness at different gas pressures. Experimental results for hystrersis loops are used to: (i) compare with the theoretical results, and (ii) obtain the relation between the stiffness of RSASD and the gas pressure. Finally, shake table tests are conducted using an almost full-scale 3-storey steel frame model equipped with full-scale RSASDs to show their performance in reducing the building responses. For the experimental results presented in this paper, emphasis is placed on the near-field earthquakes, including El Centro, Kobe and Chi-Chi earthquakes. Experimental results demonstrate the performance of RSASDs in reducing the responses of the building model subject to several near-field earthquake records. All tests presented herein were conducted using large shake table facilities at the National Center for Research on Earthquake Engineering (NCREE) in Taipei, Taiwan.

2. PRELIMINARIES

The RSASD consists of a hydraulic cylinder–piston system with a valve in the bypass pipe connecting two sides of the cylinder, as shown in Figure 1. When the valve is closed, the damper serves as a stiffness element in which the stiffness K_{fi} is provided by the bulk modulus of the

DOI: 10.1002/eqe

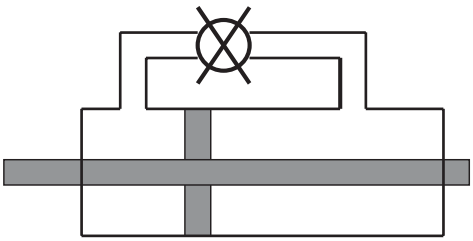

Figure 1. Schematic diagram of the semi-active stiffness damper (SASD).

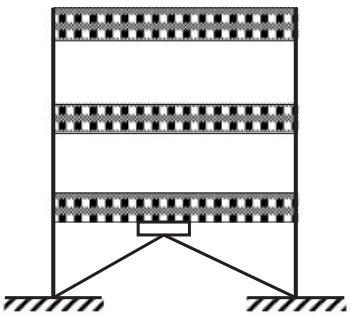

Figure 2. A three-storey building model equipped with RSASD.

fluid or pressurized gas in the cylinder. When the valve is open, the piston is free to move and the damper provides only a very small level of damping without stiffness. For applications to structural control, such as the reduction of the building response subject to an earthquake, the RSASD in Figure 1 will be connected to a symmetric bracing and installed in selected storey units, as shown in Figure 2. In Figure 2, the hydraulic/pneumatic cylinder of RSASD is fixed to the bracing, and the piston is connected to the upper floor. Hence, the RSASD and the bracing are connected in series. The assembly of the RSASD and the bracing, referred to as the RSASD–bracing system, is connected in parallel with the storey frame, and therefore the inter-storey drift results in a control force from the RSASD–bracing system.

If the horizontal stiffness of the symmetric bracing in the ith storey unit is denoted by K_{bi}, then the effective stiffness of the entire RSASD–bracing system in the ith storey unit, denoted by K_{hi}, is given by

$$K_{hi} = K_{fi} K_{bi} / (K_{fi} + K_{bi}) \tag{1}$$

because K_{fi} and K_{bi} are connected in series. The entire RSASD–bracing system described above can operate in either passive or semi-active modes. In the passive operation, the valve is either always open or closed. When the valve is always closed, the device adds a constant stiffness K_{hi} to the ith storey unit. On the other hand, when the valve is always open, the device adds a very small amount of damping to the structure.

For the semi-active control operation, two distinctive control modes can be used; namely, resetting and switching. For the resetting control mode, the valve is always closed; hence, the energy is stored continually in the damper–bracing system in terms of the potential energy during

DOI: 10.1002/eqe

vibration. At appropriate time instants, the valve is pulsed to open and close quickly. The opening of the valve releases the energy stored in the damper system through sloshing. Once the fluid is settled, the valve is closed (or reset), referred to as resetting. Right after resetting, the pressures in both chambers of the cylinder are equal and hence the control force of the RSASD is zero. Hence, by pulsing the valve at appropriate time instants, energy can be drawn from the vibrating system to reduce the structural response. The entire damper–bracing system operating in the resetting mode is referred to as the RSASD system. The second semi-active control mode is to open the valve of the damper during a certain time interval and to close it during another time interval, referred to as the switching control. Such an on–off switching control system, referred to as the switching semi-active stiffness damper (SSASD), is conceptually identical to the active variable stiffness (AVS) system proposed by Kobori *et al.* [17].

Let x_i be the inter-storey drift of the ith storey unit in which the RSASD–bracing system is installed, see Figure 2, and $\ddot{x}_0$ be the earthquake ground acceleration. Based on the Lyapunov stability theorem, a general control law for the RSASD–bracing system has been derived as follows [15]:

$$\text{Resetting when } \dot{x}_i + \alpha x_i + \beta \ddot{x}_0 = 0 \tag{2}$$

in which α and β are some constants. For practical applications, a special case of interest is to set $\alpha = \beta = 0$, i.e.

$$\text{Resetting when } \dot{x} = 0 \tag{3}$$

This control law was also derived based on the condition that under sinusoidal excitations resetting occurs when the energy stored in RSASD is maximum [13, 14], and it will be used in this paper.

For the switching operation or AVS (or SSASD), a control law has been proposed by Kamagata and Kobori [18] as

$$\begin{gathered}\text{Valve closed when } x_i \dot{x}_i \geqslant 0 \\ \text{Valve opened when } x_i \dot{x}_i < 0\end{gathered} \tag{4}$$

The control law in Equation (4) has also been derived based on the sliding mode control [19].

Note that the drift x_i and its velocity $\dot{x}_i$ across the damper can be measured using sensors embedded in the damper. It is observed from Equations (2)–(4) that the control laws above are completely decentralized. The main advantage of the decentralized control is that the control force from a given damper does not depend on the response at other locations of the structure, so that it is robust with respect to the uncertainty of the structural properties.

The capacity of a control device may be reflected by its hysteretic behaviour, e.g. the hysteresis loop. For a given damper stiffness K_{fi}, the theoretical hysteresis loop for the RSASD based on the control law in Equation (3) is presented in Figure 3(a), whereas that of the AVS (or SSASD) based on the control law in Equation (4) is shown in Figure 3(b), also see [19]. In Figure 3, the slope of the hysteresis loop is K_{fi}. The area under the hysteresis loop is the energy dissipated by the damper per cycle of displacement. As observed from Figures 3(a) and (b), the energy dissipation capacity of the RSASD is much larger than that of the AVS (or SSASD). This fact has also been demonstrated through extensive numerical simulation results [15]. Experimental

DOI: 10.1002/eqe

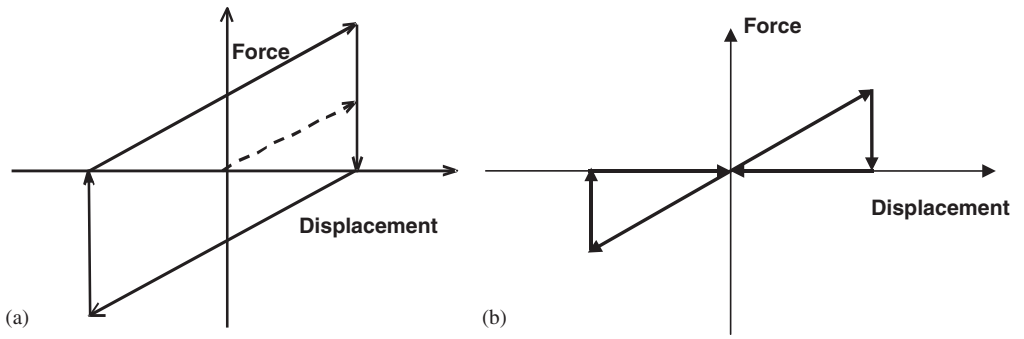

Figure 3. Hysteresis loops for: (a) RSASD and (b) AVS (SSASD).

results for hysteresis loops of the full-scale RSASD will be compared with the theoretical results, Figure 3, later.

3. HARDWARE IMPLEMENTATION OF RSASD

In this paper, the prototype RSASD devices are pneumatic, employing pressurized nitrogen. As discussed in [14] and further verified by shaking table tests here, the force produced by the damper can be approximated by that of a linear spring with stiffness

$$K_{fi} = (2A^2 K p_0)/v_0 \tag{5}$$

in which A is the piston area, p_0 is the initial gas pressure, v_0 is the initial volume, and K is the ratio of constant pressure specific heat of the gas to the constant volume specific heat of the gas. For small motion approximation, it can be assumed that v_0 is equal on both sides of the piston. Hence, the stiffness K_{fi} is linearly related to the gas pressure p_0. While Equation (5) provides an approximate formula for computing the theoretical value of the stiffness of RSASD, the actual stiffness of RSASD in applications is determined through experimental tests. This is because the stiffness is also influenced by the uncertainties of the design and manufacturing of hardware, and it is easy to perform experimental tests as will be shown below.

The hardware implementation of this device is shown in Figure 4. The cylinder is a Parker hydraulic cylinder capable of a peak pressure of 5000 psi (34.4 MPa) with a 4 in (10.16 cm) bore and a ± 1.5 in (± 3.81 cm) stroke. The piston area is $10\,\text{in}^2$ ($64.516\,\text{cm}^2$). The valve connecting the two sides of the cylinder is a Moog direct drive proportional valve capable of less than 5 ms response time with the orifice area proportional to the control voltage. The valve is connected to a 24 V ordinary battery for the power supply for resetting. Both sides of the hydraulic cylinder were filled with nitrogen gas up to about $p_0 = 800$ psi (5.516 MPa). Note that typical hydraulic cylinders can handle up to a maximum of about 3000 psi (20.7 MPa) easily, so that a peak force level of about 30 000 pounds (133.4 kN) can be achieved with a piston area of $10\,\text{in}^2$. In this device, a micro-controller is used for implementing the control law in Equation (3), so that the entire unit is self-sufficient without the need of a computer.

DOI: 10.1002/eqe

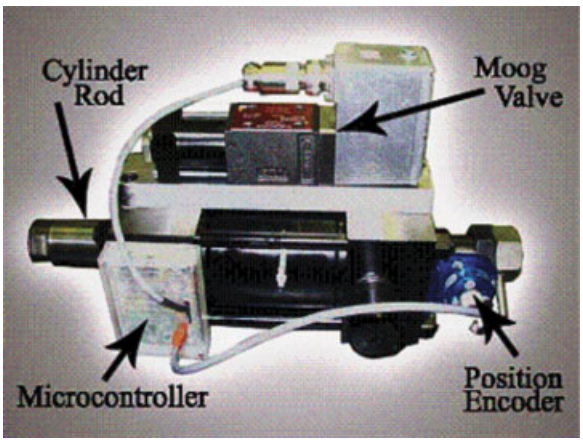

Figure 4. Resetable semi-active stiffness damper.

4. EXPERIMENTAL VERIFICATION FOR HYSTERESIS LOOPS

Two large-scale RSASDs, with the specifications discussed above, have been connected to a large actuator for testing the hysteretic behaviour as shown in Figure 5. Each RSASD has a peak stroke of ± 3.8 cm, a peak force of 40 kN and a maximum gas pressure of 720 psi (4.964 MPa). An RSASD is subject to a sinusoidal displacement at 0.5 Hz with the amplitude of 10 mm as shown in Figure 6(a). Based on the control law in Equation (3), the control force from the RSASD is measured and shown in Figure 6(b) for a gas pressure of 300 psi (2.07 MPa). It is observed from Figures 6(a) and (b) that resetting occurs at zero velocity, i.e. at either peak or trough of Figure 6(a). From Figures 6(a) and (b), the force–displacement relation (i.e. the hysterersis loop) for the RSASD can be constructed as shown in Figure 6(c). Experimental tests have been conducted for both RSASDs with different gas pressures ranging from 0 to 700 psi (4.83 MPa) at an interval of 100 psi. Due to space limitations, only the results for gas pressures at 300, 500 and 700 psi (4.83 MPa) of the 1st RSASD are presented in Figures 6–8. All the tests presented above have been conducted up to 50 cycles. For clarity of presentation, only the results for the first 10 cycles are presented in Figures 6–8.

It is observed from these figures that the experimental hysteresis loops correlate qualitatively with that of the theoretical ones, e.g. Figure 3(a). Note that the scales of the vertical axis in Figures 6(c), 7(c) and 8(c) are different. In fact, the area under the hysteresis loop is larger when the gas pressure is larger, which is expected since higher pressure leads to larger stored energy for release at each resetting. From the experimental hysteresis loop, the stiffness K_{fi} of the RSASD, which is the slope of the hysteresis loop, can be determined, referred to as the semi-active stiffness. The stiffness thus obtained is presented in Figure 9(a) for different gas pressures as dots. A linear regression line has been obtained based on the experimental results (dots) and presented in Figure 9(a).

Experimental tests have also been conducted for cases in which: (i) the valve is always closed, and (ii) the valve is always open. When the valve is always closed, the stiffness of the RSASD can easily be obtained from the experimental results, referred to as the passive stiffness. The test results for the passive stiffness K_{fi} *versus* the gas pressure for the 1st RSASD are presented in

DOI: 10.1002/eqe

Figure 5. RSASD connected to an actuator.

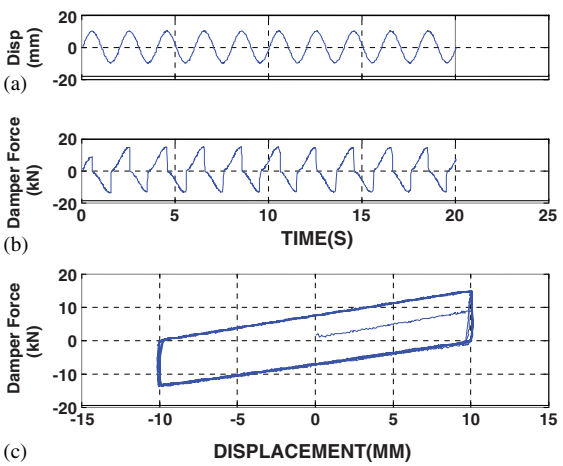

Figure 6. Test results of RSASD with gas pressure = 300 psi (2.07 MPa): (a) sinusoidal displacement; (b) damper force; and (c) hysteresis loop.

Figure 9(b) as dots. Also shown in the figure as a straight line is the linear regression fit. It is observed from Figures 9(a) and (b) that the difference between the semi-active stiffness and the passive stiffness is small and that the stiffness K_{fi} of the RSASD is linearly related to the gas pressure p_0 as presented in Equation (5). It is mentioned that we have tested 2 RASADs, and the test results for the 2nd RSASD are very close to that of the 1st RSASD presented herein. Tests for the hysteresis loops at different frequencies, e.g. 1, 1.5, 2.0 and 2.5 Hz, have been conducted, and all

DOI: 10.1002/eqe

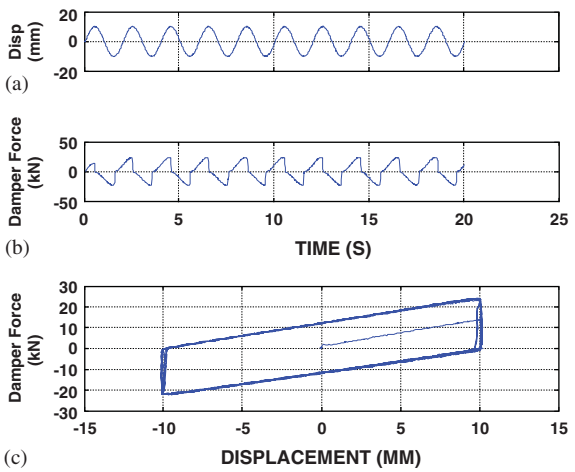

Figure 7. Test results of RSASD with gas pressure = 500 psi (3.45 MPa): (a) sinusoidal displacement; (b) damper force; and (c) hysteresis loop.

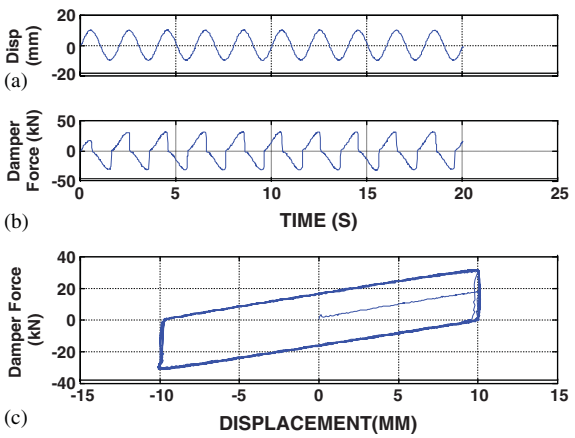

Figure 8. Test results of RSASD with gas pressure = 700 psi (4.83 MPa): (a) sinusoidal displacement; (b) damper force; and (c) hysteresis loop.

the test results yield the same hysteresis loops. Likewise, tests for the hysteresis loops at different amplitudes, e.g. 15 mm, have also been conducted. The resulting stiffness is identical irrespective to the displacement amplitudes, and the resulting hysteresis loops are just scaled linearly from that presented in Figures 6(c)–8(c), as expected. Due to space limitation, these scaled hysteresis loops are not presented. Finally, a slight increase of temperature in RSASD during the tests has been observed; unfortunately, however, it is not monitored since it did not appear to be substantial.

DOI: 10.1002/eqe

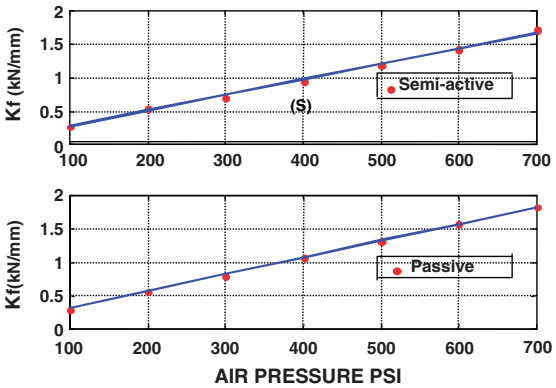

Figure 9. Damper stiffness *versus* gas pressure (1 psi = 6.895 kPa): (a) semi-active stiffness and (b) passive stiffness (valve always on).

5. FULL-SCALE SHAKE TABLE TESTS

In the literature, it has been observed that passive control devices alone may not be effective for near-field earthquakes and the protection of structures subject to such detrimental earthquakes is of great concern. Hence, the goal of this paper is to experimentally assess the effectiveness of RSASDs in reducing the structural response subject to detrimental near-field earthquakes. Note that the effectiveness of RSASDs for all types of earthquakes, including near-field and far-field earthquakes, has been evaluated through numerical simulation studies (e.g. [9, 15, 16]).

To demonstrate the performance of RSASDs in reducing the building response subject to near-field earthquakes, shake table tests of an almost full-scale 3-storey steel frame building model equipped with RSASDs presented above have been conducted at the National Center for Research on Earthquake Engineering (NCREE), Taipei, Taiwan. The building model is 3 m by 2 m with 9 m height (3 m per storey) as shown in Figure 10. The mass of each floor is 6540 kg, including the inverted triangular bracings, and the first natural frequency is 1 Hz. Various near-field earthquakes, including Kobe, Chi-Chi and El Centro earthquakes, have been applied in the 3-m direction, and these earthquakes have been scaled to a PGA of 100 gales as shown in Figure 11. The reason for scaling the PGA of all earthquakes used to 100 gales is to ensure that the 3-storey test frame stays within the linear elastic range. Each floor is installed with two displacement sensors, two velocity sensors, and two acceleration sensors. The two acceleration sensors on each floor are installed at the front and back edges of the floor, and the floor acceleration is obtained by the average of the readings from these two sensors. The same situation holds for velocity and displacement sensors. From the sensor measurements, important response quantities, including the inter-storey drifts, $d_1(t)$, $d_2(t)$, and $d_3(t)$, and the absolute floor accelerations, $a_1(t)$, $a_2(t)$, and $a_3(t)$, are obtained. For simplicity of presentation, the dependence on 't' of these quantities will be dropped in the following.

Without control device, the response quantities of the building model, including the inverted bracing systems, have been recorded for comparison. Consider the case in which only one RSASD with a gas pressure of 280 psi (1.932 MPa) is installed in the first storey, as shown in Figure 12. The test results for the inter-storey drifts, d_1, d_2, and d_3, of the building under the Chi-Chi TCU076

DOI: 10.1002/eqe

Figure 10. Three-storey large-scale frame model on shake table.

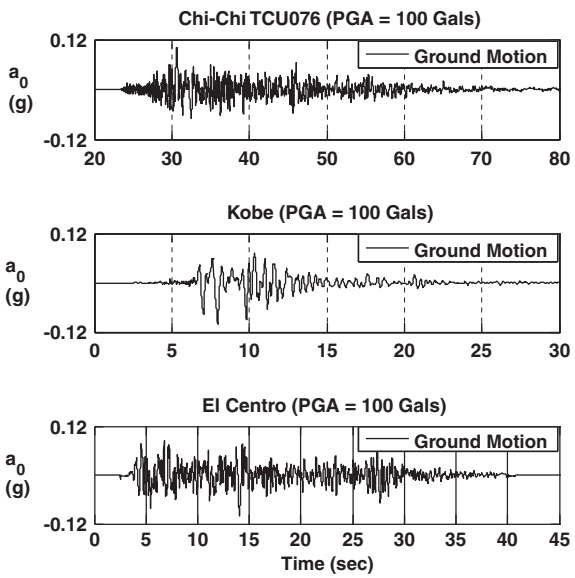

Figure 11. Ground acceleration used for shake table tests (PGA scaled to 100 Gals).

DOI: 10.1002/eqe

Figure 12. A RSASD installed in the first storey.

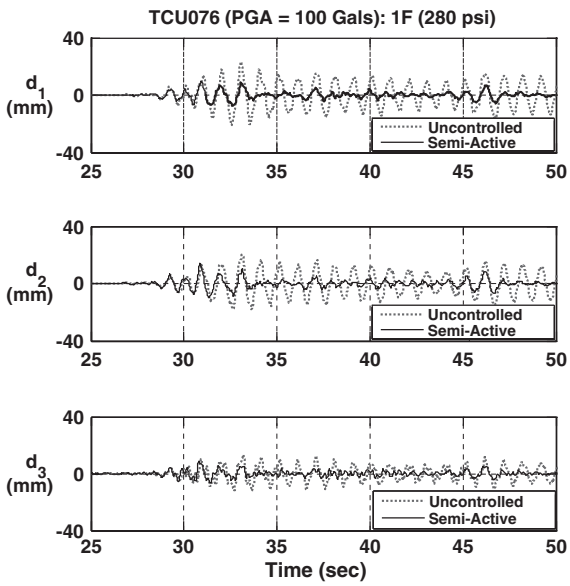

Figure 13. Inter-storey drifts under Chi-Chi TCU076 earthquake: one RSASD with gas pressure $p_1 = 280\,\text{psi}$ in first storey.

earthquake are presented in Figure 13 as solid curves and denoted by 'semi-active'. Also shown in Figure 13 as dotted curves are the corresponding experimental results without control. Further, the absolute accelerations of all floors, a_1, a_2, and a_3, are presented in Figure 14, in which the solid curves are the responses with control and the dotted curves are that without control. It is observed from Figures 13 and 14 that the RSASD is more effective in reducing the inter-storey drifts than the floor accelerations of the building.

DOI: 10.1002/eqe

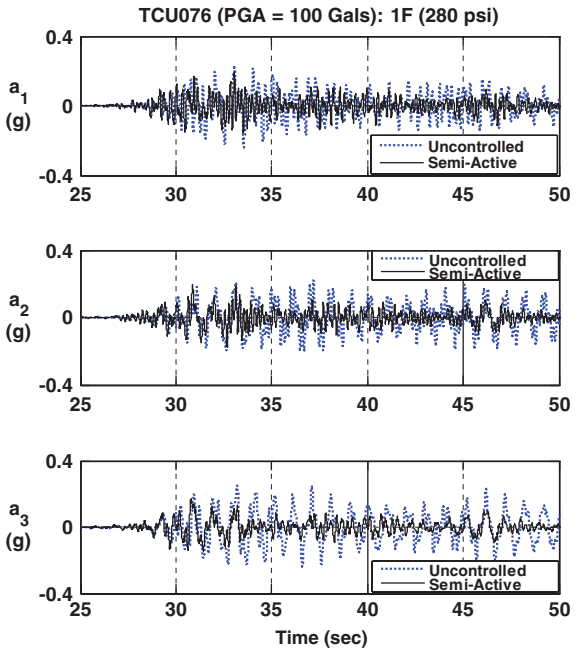

Figure 14. Floor accelerations under Chi-Chi TCU076 earthquake: one RSASD with gas pressure $p_1 = 200$ psi in first storey.

Tests have also been conducted when the valve of the device is always closed, in this case the device only adds the stiffness K_{hi} to the first storey unit, referred to as braced control. In general, braced control is not as effective as the semi-active control. In addition to the response time histories, such as Figures 13 and 14, important response quantities are the peak inter-storey drift of each storey and the peak acceleration of each floor. Likewise, the root mean square (RMS) values of these inter-storey drifts and floor accelerations are also important measures of the performance of the control device. These peak and RMS values of the response quantities are summarized in Columns (6)–(7) of Table I, where the structure is subject to the Chi-Chi TCU076 earthquake, and only one control device is installed in the first storey with a gas pressure of 280 psi (1.932 MPa), denoted by $p_1 = 280$ psi. Also shown in Columns (2)–(5) of Table I for comparison are the corresponding response quantities for: (i) the structure without control, and (ii) the structure with braced control in the first storey.

It is mentioned that the stiffness of the bracing K_{bi} is much bigger than that of the damper K_{fi}, and hence the stiffness of the RSASD–bracing system K_{hi} is approximately equal to the stiffness of the damper, i.e. $K_{hi} \approx K_{fi}$, see Equation (1). Also, in computing the RMS value of a response quantity, only a segment of significant response in (t_1, t_2) of the uncontrolled inter-storey drift of the first storey is considered. t_1 is chosen when the response $d_1(t_1)$ is 10% of the absolute peak response and t_2 corresponds to the local peak (or trough) that is approximately 10% of the absolute peak response. Thus, $t_1 = 28.70$ s and $t_2 = 76.36$ s for the Chi-Chi TCU076 earthquake, $t_1 = 41.85$ s and $t_2 = 46.08$ s for the El Centro earthquake, and $t_1 = 4.540$ s and $t_2 = 40.77$ s for the Kobe earthquake.

DOI: 10.1002/eqe

Table I. Experimental results for peak and RMS responses for ChiChi TCU076 earthquake.

			One RSASD $p_1 = 280$ psi				One RSASD $p_1 = 325$ psi			
	Uncontrolled		Braced		Semi-active		Braced		Semi-active	
(1)	Peak (2)	RMS (3)	Peak (4)	RMS (5)	Peak (6)	RMS (7)	Peak (8)	RMS (9)	Peak (10)	RMS (11)
d_1 (mm)	23.33	6.724	15.84	2.934	9.86	1.882	14.94	2.417	8.44	1.675
d_2 (mm)	20.49	6.263	18.33	3.630	14.36	2.266	18.82	3.223	13.73	2.122
d_3 (mm)	12.85	3.935	13.31	2.914	8.43	1.564	13.23	2.369	7.76	1.471
a_1 (g)	0.239	0.060	0.292	0.069	0.190	0.032	0.247	0.046	0.236	0.032
a_2 (g)	0.222	0.060	0.241	0.069	0.194	0.032	0.235	0.046	0.194	0.032
a_3 (g)	0.250	0.075	0.263	0.061	0.171	0.031	0.269	0.048	0.162	0.030

			Two RSASDs $p_1 = 280$ psi, $p_2 = 280$ psi				Two RSASDs $p_1 = 280$ psi, $p_2 = 420$ psi			
	Uncontrolled		Braced		Semi-active		Braced		Semi-active	
(1)	Peak (2)	RMS (3)	Peak (12)	RMS (13)	Peak (14)	RMS (15)	Peak (16)	RMS (17)	Peak (18)	RMS (19)
d_1 (mm)	23.33	6.724	13.23	2.470	9.72	1.725	14.31	2.709	13.11	1.739
d_2 (mm)	20.49	6.263	14.78	2.215	10.86	1.628	14.49	2.224	8.35	1.448
d_3 (mm)	12.85	3.935	17.15	2.375	12.22	1.480	18.32	2.598	12.68	1.518
a_1 (g)	0.239	0.060	0.230	0.043	0.196	0.031	0.234	0.047	0.218	0.032
a_2 (g)	0.222	0.060	0.207	0.043	0.214	0.031	0.249	0.047	0.243	0.032
a_3 (g)	0.250	0.075	0.365	0.051	0.267	0.031	0.383	0.056	0.269	0.033

			Two RSASDs $p_1 = 280$ psi, $p_3 = 280$ psi			
	Uncontrolled		Braced		Semi-active	
(1)	Peak (2)	RMS (3)	Peak (20)	RMS (21)	Peak (22)	RMS (23)
d_1 (mm)	23.33	6.724	15.27	2.477	11.59	1.919
d_2 (mm)	20.49	6.263	20.53	3.203	14.93	2.345
d_3 (mm)	12.85	3.935	8.41	1.404	9.32	1.154
a_1 (g)	0.239	0.060	0.124	0.023	0.235	0.028
a_2 (g)	0.222	0.060	0.257	0.023	0.222	0.028
a_3 (g)	0.250	0.075	0.229	0.037	0.227	0.030

The performance of the RSASD depends on its effective stiffness, K_{hi} (or the gas pressure). Here, we increase the gas pressure to $p_1 = 325$ psi, and the test results for the peak and RMS values are presented in Columns (8)–(11) of Table I. The results shown in Columns (4)–(11) of Table I indicate that the performance in reducing the inter-storey drifts improves for $p_1 = 325$ psi over that for $p_1 = 280$ psi. However, the performance for the reduction of acceleration responses is almost identical. With only one RSASD installed in the first storey, experimental results for the peak and RMS values of the response quantities for: (i) the El Centro earthquake with $p_1 = 325$ psi and

DOI: 10.1002/eqe

Table II. Experimental results for peak and RMS responses for El Centro earthquake.

			One RSASD $p_1 = 325$ psi				One RSASD $p_1 = 550$ psi			
	Uncontrolled		Braced		Semi-active		Braced		Semi-active	
(1)	Peak (2)	RMS (3)	Peak (4)	RMS (5)	Peak (6)	RMS (7)	Peak (8)	RMS (9)	Peak (10)	RMS (11)
d_1 (mm)	15.08	4.549	7.90	1.963	8.23	1.473	6.69	1.404	7.21	1.006
d_2 (mm)	13.49	3.327	11.41	2.680	9.10	1.791	12.29	2.543	9.45	1.784
d_3 (mm)	13.65	4.771	8.81	1.853	8.44	1.319	10.29	1.764	8.15	1.307
a_1 (g)	0.308	0.134	0.139	0.031	0.145	0.029	0.135	0.029	0.169	0.028
a_2 (g)	0.213	0.134	0.148	0.031	0.177	0.029	0.188	0.029	0.183	0.028
a_3 (g)	0.282	0.107	0.174	0.036	0.178	0.027	0.210	0.035	0.189	0.027

			Two RSASDs $p_1 = 280$ psi, $p_2 = 280$ psi				Two RSASDs $p_1 = 280$ psi, $p_2 = 420$ psi			
	Uncontrolled		Braced		Semi-active		Braced		Semi-active	
(1)	Peak (2)	RMS (3)	Peak (12)	RMS (13)	Peak (14)	RMS (15)	Peak (16)	RMS (17)	Peak (18)	RMS (19)
d_1 (mm)	15.08	4.549	11.69	2.483	7.30	1.406	11.37	2.626	7.09	1.296
d_2 (mm)	13.49	3.327	10.16	2.302	6.90	1.288	9.71	2.229	5.85	1.096
d_3 (mm)	13.65	4.771	9.60	2.170	6.85	1.215	9.26	2.242	5.92	1.128
a_1 (g)	0.308	0.134	0.131	0.031	0.158	0.025	0.138	0.030	0.152	0.024
a_2 (g)	0.213	0.134	0.162	0.031	0.164	0.025	0.161	0.030	0.152	0.024
a_3 (g)	0.282	0.107	0.190	0.044	0.148	0.026	0.191	0.046	0.136	0.024

			Two RSASDs $p_1 = 280$ psi, $p_3 = 280$ psi			
	Uncontrolled		Braced		Semi-active	
(1)	Peak (2)	RMS (3)	Peak (20)	RMS (21)	Peak (22)	RMS (23)
d_1 (mm)	15.08	4.549	9.51	2.058	12.20	1.711
d_2 (mm)	13.49	3.327	11.92	2.670	11.89	2.024
d_3 (mm)	13.65	4.771	6.70	1.215	6.98	0.996
a_1 (g)	0.308	0.134	0.116	0.024	0.219	0.028
a_2 (g)	0.213	0.134	0.135	0.024	0.175	0.028
a_3 (g)	0.282	0.107	0.186	0.032	0.220	0.026

$p_1 = 550$ psi, and (ii) the Kobe earthquake with $p_1 = 280$ psi are presented in Columns (4)–(11) of Tables II and III, respectively. Also shown in Columns (2)–(3) of these tables are the experimental results of the uncontrolled structure. These experimental results indicate that the performance of RSASD in reducing the inter-storey drifts improves for $p_1 = 325$ psi over that for $p_1 = 280$ psi, whereas the performance for the reduction of acceleration responses remains about the same.

Given the test results presented above for the case of one RSASD device installed in the first storey (see Tables I–III), the performance of RSASD for reducing the peak inter-storey drifts,

DOI: 10.1002/eqe

Table III. Experimental results for peak and RMS responses for Kobe earthquake.

			One RSASD $p_1 = 280$ psi			
	Uncontrolled		Braced		Semi-active	
(1)	Peak (2)	RMS (3)	Peak (4)	RMS (5)	Peak (6)	RMS (7)
d_1 (mm)	17.47	5.741	12.28	2.554	12.03	1.752
d_2 (mm)	15.33	5.287	19.57	3.424	16.86	2.244
d_3 (mm)	10.32	3.571	12.54	2.187	11.23	1.527
a_1 (g)	0.165	0.060	0.169	0.022	0.184	0.026
a_2 (g)	0.187	0.060	0.166	0.022	0.196	0.026
a_3 (g)	0.198	0.070	0.247	0.041	0.229	0.030

			Two RSASDs $p_1 = 280$ psi, $p_2 = 420$ psi			
	Uncontrolled		Braced		Semi-active	
(1)	Peak (2)	RMS (3)	Peak (12)	RMS (13)	Peak (14)	RMS (15)
d_1 (mm)	17.47	5.741	14.47	2.709	9.25	1.465
d_2 (mm)	15.33	5.287	13.60	2.224	8.54	1.361
d_3 (mm)	10.32	3.571	13.62	2.598	11.19	1.294
a_1 (g)	0.165	0.060	0.129	0.024	0.268	0.028
a_2 (g)	0.187	0.060	0.172	0.024	0.270	0.028
a_3 (g)	0.198	0.070	0.270	0.046	0.261	0.028

			Two RSASDs $p_1 = 280$ psi, $p_3 = 280$ psi			
	Uncontrolled		Braced		Semi-active	
(1)	Peak (2)	RMS (3)	Peak (20)	RMS (21)	Peak (22)	RMS (23)
d_1 (mm)	17.47	5.741	14.02	2.809	12.05	1.755
d_2 (mm)	15.33	5.287	21.19	3.726	16.68	2.213
d_3 (mm)	10.32	3.571	9.34	1.626	7.61	1.042
a_1 (g)	0.165	0.060	0.144	0.021	0.238	0.026
a_2 (g)	0.187	0.060	0.184	0.021	0.181	0.026
a_3 (g)	0.198	0.070	0.254	0.043	0.288	0.028

d_1, d_2, and d_3, is impressive. On the other hand, the performance for reducing the peak floor accelerations, a_1, a_2, and a_3, is not particularly impressive. However, the performance of RSASD for the reduction of RMS values is quite significant not only for the inter-storey drifts but also for the floor accelerations.

The performance of any control system depends on the number of controllers used. Here, tests have been conducted by installing one RSASD in the first storey with a gas pressure p_1 and another RSASD in the second storey with a gas pressure p_2. Test results for the inter-storey drifts

DOI: 10.1002/eqe

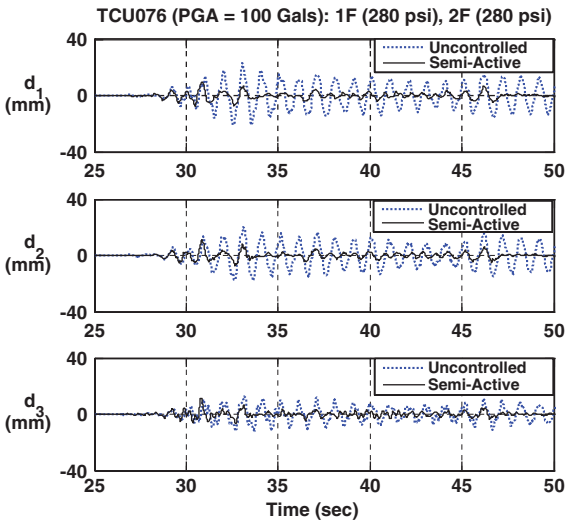

Figure 15. Inter-storey drifts under Chi-Chi TCU076 earthquake: one RSASD with gas pressure $p_1 = 280$ psi in first storey and one RSASD with gas pressure $p_2 = 280$ psi in second storey.

with $p_1 = 280$ psi and $p_2 = 280$ psi for the Chi-Chi TCU076 earthquake are presented in Figure 15 as solid curves, whereas the dotted curves are the test results without control. Peak and RMS values for inter-storey drifts and absolute floor acceleration are presented in Columns (12)–(19) of Table I for different gas pressures in each RSASD. For Kobe and El Centro earthquakes, test results for the inter-storey drifts with $p_1 = 280$ psi and $p_2 = 420$ psi are presented as solid curves in Figures 16 and 17, respectively, whereas the dotted curves are the test results without control. Peak and RMS values of the response quantities for the El Centro earthquake are shown in Columns (12)–(19) of Table II for RSASDs with different gas pressures p_1 and p_2. For Kobe earthquake, the corresponding peak and RMS values are shown in Columns (12)–(15) of Table III. It is observed from Figures 13–17 and Tables I–III that the control performance further improves, when 2 RSASDs (one in the first storey and another in the second storey) are used, in comparison with the control performance using only one RSASD in the first storey.

Finally, the performance of the control devices depends also on the location of the controllers. Now, we install one RSASD in the first storey with $p_1 = 280$ psi and another RSASD in the third storey with $p_3 = 280$ psi, where no device is installed in the second storey. Experimental test results for the peak and RMS values of the response quantities are summarized and presented in Columns (20)–(23) of Tables I–III for different earthquake excitations. Due to space limitations, time histories for the inter-storey drifts are not presented. A comparison of the present results, Columns (20)–(23) of Tables I–III, with that of the previous case using two RSASDs, Columns (12)–(19) of Tables I–III, indicates that the control performance of the previous architecture, i.e. one RSASD in the first storey and another in the second, is better.

The following conclusions are obtained through a careful evaluation of the test results presented in Figures 11–17 and Tables I–III: (i) the full-scale RSASD is quite effective in reducing the inter-storey drifts, including the peak drifts and RMS values, of the building subject to several near-field earthquakes that were examined; (ii) the RSASD is less effective in reducing the peak floor acceleration, but it is quite effective in reducing the RMS values of the floor acceleration;

DOI: 10.1002/eqe

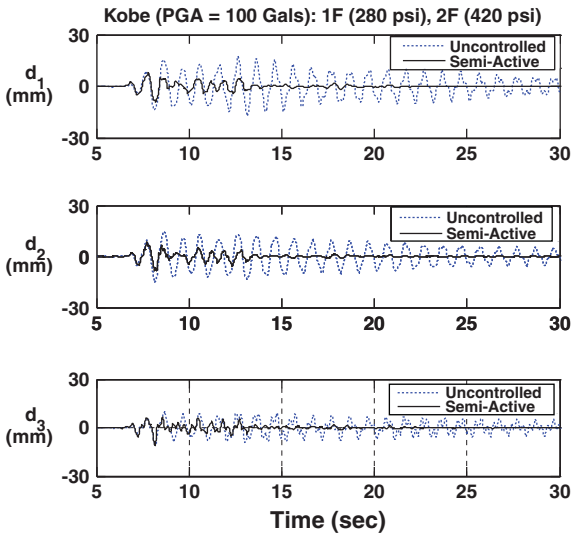

Figure 16. Inter-storey drifts under Kobe earthquake: one RSASD with gas pressure $p_1 = 280$ psi in first storey and one RSASD with gas pressure $p_2 = 420$ psi in second storey.

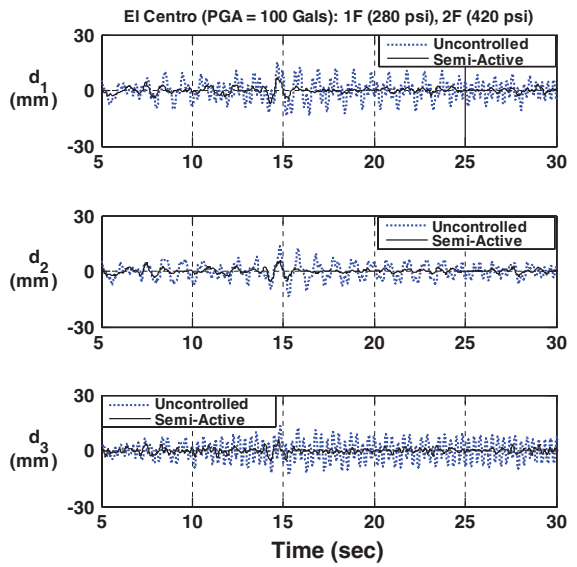

Figure 17. Inter-storey drifts under El Centro earthquake: one RSASD with gas pressure $p_1 = 280$ psi in first storey and one RSASD with gas pressure $p_2 = 420$ psi in second storey.

(iii) the performance of RSASD depends on the number of RSASDs used as well as their locations of installation; and (iv) the performance of RSASD depends on the particular earthquake excitation used.

DOI: 10.1002/eqe

6. CONCLUSION

Full-scale resetable semi-active stiffness dampers (RSASDs) developed and designed at UCI for applications to seismic hazard mitigations of structures have been manufactured and tested. Instead of the hydraulic fluid, the pressurized gas has been used, so that the stiffness of the RSASD can be adjusted easily by changing the gas pressure. Experimental tests have been conducted to obtain the hysteresis loops of the RSASDs, representing the energy dissipation capacity of the control device. It is demonstrated that the experimental hysteresis loops of RSASD correlated well qualitatively with those of the theoretical ones. Experimental data further indicate that the stiffness of the RSASD is linearly related to the gas pressure, as expected.

Shake table tests of an almost full-scale building model equipped with large-scale RSASDs have been conducted. Various configurations for the installation of RSASDs have been tested, including different number of RSASDs used, different stiffness (or gas pressure) of RSASDs, and different damper locations. Experimental results demonstrate that the full-scale RSASD is quite effective in reducing the inter-storey drifts of the building, including the peak drifts and RMS values, subject to several near-field earthquakes that were examined. However, the performance of RSASDs in reducing the peak floor accelerations is less effective, but the reduction of the RMS floor accelerations is quite significant. Typically, the performance of RSASDs in reducing the building responses depends on the particular architecture for the installation of RSASDs, including the number of RSASDs used, the magnitude of RSASD's stiffness (or gas pressure), and the location of RSASD. In practical applications, for a given structure (building), an important task is to determine the optimal number of controllers (e.g. RASADs) and their corresponding optimal locations and capacity (or stiffness). In this connection, the methods described in, e.g. [22–24] may be used.

In comparison with other semi-active control devices, for instance, the popular MR dampers, the RSASD device has advantages in its simplicity. This is because the device consists of a hydraulic cylinder and a valve, which are standard mechanical components available readily and inexpensively. Likewise, the control law is quite simple and decentralized as well as robust with respect to structural uncertainties. Consequently, the system reliability and total cost of the RSASD compare favourably with any other semi-active control systems.

It is well-known that passive energy dissipation devices have advantages over the semi-active control devices in terms of cost, reliability, maintainability, etc. If properly tuned, passive devices also have plausible performance in dissipating energies. Based on previous experience, e.g. [4], passive devices, if properly tuned, perform well in comparison with semi-active devices. However, a proper tuning of the passive devices depends on the particular earthquake excitation. In practice, the future earthquake is unknown and passive devices have no ability to adapt to the changing external loads. On the other hand, semi-active devices have capability to adapt to changing external excitations through their control laws, and hence their performance is more robust. In this connection, simulation studies for the performance evaluations of RSASD and other passive devices have been conducted using two different benchmark problems [9, 25]. Finally, for a specific practical application, studies are needed to evaluate the benefits and drawbacks of different passive and semi-active control devices.

ACKNOWLEDGEMENTS

This work is partially supported by the US National Science Foundation through grant CMS-0218813.

DOI: 10.1002/eqe

REFERENCES

1. Spencer BF, Nagarajaiah S. State of the art of structural control. *Journal of Structural Engineering* (ASCE) 2003; **129**(7):845–856.
2. Nagarajaiah S, Spencer BF, Yang JN. Recent advances in control of civil infrastructures in U.S.A. *Proceedings US-Korea Joint Seminar/Workshop on Smart Structures Technologies*. Korea Techno-Press: Seoul, Korea, 2004; 3–17.
3. Kawashima K, Unjoh S. Seismic response control of bridges by variable dampers. *Journal of Structural Engineering* (ASCE) 1994; **120**(9):2583–2601.
4. Yang JN, Wu JC, Kawashima K, Unjoh S. Hybrid control of seismic-excited bridge structures. *Earthquake Engineering and Structural Dynamics* 1995; **24**(11):1437–1451.
5. Patten W, Sun J, Li G, Kuehn J, Song G. Field test of an intelligent stiffener for bridges at the I-35 Walnut Creek bridge. *Earthquake Engineering and Structural Dynamics* 1999; **28**(2):109–126.
6. Kurata N, Kobori T, Takahashi M, Niwa N, Midorikawa H. Actual seismic response controlled building with semi-active damper system. *Earthquake Engineering and Structural Dynamics* 1999; **28**(11):1427–1447.
7. Spencer BF, Sain MK. Controlling Buildings: a new frontier in feedback. *Special Issue of the IEEE Control Systems Magazine on Emerging Technology* 1997; **17**(6):19–35.
8. He WL, Agrawal AK, Yang JN. A novel semi-active friction controller for linear structures against earthquakes. *Journal of Structural Engineering* (ASCE) 2003; **129**(7):941–950.
9. Agrawal AK, Yang JN, He WL. Applications of some semi-active control systems for a benchmark cable-stayed bridge. *Journal of Structural Engineering* (ASCE) 2003; **129**(7):884–894.
10. Chen GD. Towards an integrated and maintenance-free semi-active control system with uninterruptible power sources. *Proceedings of the 4th International Workshop on Structural Control*, Columbia University, NY, 2004.
11. Nasu T, Kobori T, Takahashi M, Niwa N, Ogasawara K. Active variable stiffness system with non-resonant control. *Earthquake Engineering and Structural Dynamics* 2001; **30**(10):1597–1614.
12. Nagarajaiah S, Saharabudhe S. Seismic response control of smart sliding isolated buildings using variable stiffness systems: an experimental and numerical study. *Journal of Earthquake Engineering and Structural Dynamics* 2006; **35**(2):177–197.
13. Bobrow JE, Jabbari F, Thai K. A new approach to shock isolation and vibration suppression using a resetable actuator. *Transactions*, *Dynamic Systems*, *Measurement and Control* (ASME) 2000; **122**:570–573.
14. Jabbari F, Bobrow JE. Vibration suppression with a resetable device. *Journal of Engineering Mechanics* (ASCE) 2002; **128**(9):916–924.
15. Yang JN, Kim JH, Agrawal AK. A resetting semi-active stiffness damper for seismic response control. *Journal of Structural Engineering* (ASCE) 2000; **126**(12):1427–1433.
16. Yang JN, Agrawal AK. Semi-active hybrid control systems for nonlinear buildings against near-filed earthquakes. *Journal of Engineering Structures* 2002; **24**:271–280.
17. Kobori T, Takahashi M, Nasu T, Niwa N, Hiehata J, Ogasawara K. Seismic response controlled structure with active variable stiffness system. *Earthquake Engineering and Structural Dynamics* 1993; **22**:925–941.
18. Kamagata S, Kobori T. Autonomous adaptive control of active variable stiffness systems for seismic ground motion. *Proceedings of the 1st World Conference on Structural Control*, Los Angeles, vol. 2. USC Publications: Los Angeles, CA, 1994; TA 4–33.
19. Yang JN, Li Z, Wu JC. Control of seismic-excited buildings using active variable stiffness system. *Journal of Engineering Structures* 1996; **18**(8):589–596.
20. Nagarajaiah S. *Structural Vibration Damper With Continuously Varying Stiffness*. U.S. Patent No. 6,098,969, 2000.
21. Varadarajan N, Nagarajaiah S. Wind response control of building with variable stiffness mass damper using empirical mode decomposition and Hilbert transform. *Journal of Engineering Mechanics* (ASCE) 2004; **130**(4):451–458.
22. Yang JN, Lin S, Kim JH, Agrawal AK. Optimal design of passive energy dissipation systems based on H_∞ and H_2 performances. *Journal of Earthquake Engineering and Structural Dynamics* 2002; **31**(4):921–936.
23. Agrawal AK, Yang JN. Design of passive energy dissipation systems based on LQR methods. *Journal of Intelligent Material Systems and Structures* 1999; **10**(12):933–944.
24. Agrawal AK, Yang JN. Optimal placement of passive dampers on buildings using combinatorial optimization. *Journal of Intelligent Material Systems and Structures* 1999; **10**(12):997–1014.
25. Leavitt J, Bobrow JE, Jabbari F, Yang JN. Application of a high-pressure gas semi-active resetable damper to benchmark smart base isolated building. *Journal of Structural Control and Health Monitoring* 2006; **13**:748–757.

DOI: 10.1002/eqe